Department of Physics and Astrophysics

University of Delhi, Delhi-110007

M.Sc. Physics, Semester 4

Observational Astronomy Lab

Study of age, metallicity and extra-tidal region of a globular cluster NGC 4147

Under the supervision of

Prof. T. R. Seshadri and Dr. Sachin Pandey

Submitted By

Anisha Khatri

M.Sc. Physics (Roll No. 23026762005)

Hindu College

Department of Physics and Astrophysics

University of Delhi, Delhi

ACKNOWLEDGEMENT

I express my sincere gratitude to everyone who contributed to the successful completion of our project. This endeavor would not have been possible without the guidance, support and encouragement we received along the way.

First and foremost, I extend my heartfelt gratitude to **Prof. T. R. Seshadri and Dr. Sachin Pandey** for their invaluable guidance, constructive feedback and constant support throughout the project. Their expertise and insights have been crucial in shaping the direction of our work.

A special mention goes to my team members **Simran Kumari** and **Khushi Gupta** for their dedication, collaboration, and hard work throughout this journey. The unique contributions and commitment of each member have been instrumental in bringing this project to fruition. Thank you for your contributions and support to make this project a success.

I also thank the Department of Physics and Astrophysics, University of Delhi, for allowing me to do this project.

ABSTRACT

Galactic globular clusters (GCs) are key to improving our understanding of the formation and evolution of our Galaxy. These when explored in detail, show evidence of extra-tidal stars which are stellar bodies that end up outside the tidal radius of a cluster due to internal processes or external forces.

NGC 4147 is an old, metal-poor, and isolated globular cluster in the northern constellation of Coma Berenices. It is located around 18.5 kpc from the Sun at a relatively high galactic latitude of 77.2°. Its position makes it a candidate for association with the Sagittarius tidal stream, suggesting it may have been captured by the Milky Way after separation from the Sagittarius Dwarf Spheroidal Galaxy [1].

We aim to study the age, metallicity, and extra-tidal region of NGC 4147 using data from Gaia DR3. Extra-tidal candidates were selected based on proper motions of the cluster and the individual extra-tidal candidates, and their positions on the color–magnitude diagram. We found the cluster's age to be 13 Gyr and metallicity as −1.8 dex. A total of 14 extra-tidal candidates were identified. The presence and spatial distribution of these stars can provide insights into the past evolution of the cluster within the Milky Way.

Contents

Chapter 1

Introduction

Globular clusters (GCs) are fossil tracers of the formation and evolution of galaxies, as these are among the oldest objects in the universe. Their study provides us with key information on the dynamics of their host galaxies.

The tidal radius of a globular cluster is the distance from its center where the gravitational influence of the host galaxy (like the Milky Way) becomes stronger than the cluster's own gravity, potentially leading to stars being pulled away, and these stars are called extra-tidal stars.[2] Here, we are interested in the extra-tidal region of the globular cluster NGC 4147, studying which can provide useful insights about the different internal processes acting on the cluster itself, including stellar evolution, gas expulsion (Geyer & Burkert 2001), as well as the forces acting on the cluster which may strip stars from it.[3]

NGC 4147 is an old, metal-poor ([Fe/H] = -1.78 dex) isolated globular cluster in the northern constellation of Coma Berenices, with an apparent visual magnitude of 10.7. It is located around 60,000 light years (18.5kpc) away from the Sun at a relatively high galactic latitude of 77.2°.[4]

Our study continues in the following section as we first discuss the process of extracting the data, based on various parameters used for the analysis. In later sections, from the extracted data, we are trying to select the possible extra-tidal candidates on the basis of proper motion selection, membership probabilities, and study of color-magnitude diagram (CMD) of our cluster. Furthermore, we are plotting the density plot for the selected extra-tidal stars and trying to compute the orbit of our cluster. Finally, we discuss our results and list our final conclusions.

Chapter 2

Globular Clusters

2.1 Defining Globular Clusters

"With every passing hour our solar system comes forty-three thousand miles closer to the globular cluster M13 in the constellation Hercules, and still there are some misfits who continue to insist that there is no such thing as progress."

—Kurt Vonnegut, Jr., The Sirens of Titan (1959)

Globular clusters (GCs) are aggregates of approximately 10^4–10^6 gravitationally bound stars, highly concentrated toward the center, and typically spanning a volume from a few dozen to over 300 light-years in diameter. They resemble brilliant, ancient stellar islands orbiting the Milky Way.

As the name suggests, GCs display a largely spherical symmetry about their centers. A classic example is the globular cluster ω Centauri, often used to illustrate their densely packed nature. In the cluster's core, the stellar density can reach a few 10^3 stars per cubic light year, making it impossible to resolve individual stars from ground-based telescopes. Only with the advent of the refurbished *Hubble Space Telescope* (HST) have astronomers been able to probe into these crowded central regions, revealing stars moving randomly like gas particles under gravitational interactions. The study of GCs dates back to the dawn of modern astronomy. Since then, they have continued to provide valuable insights for astronomers and remain key benchmarks for our astrophysical understanding. Our Milky Way contains about 200 known GCs, forming a roughly spherical halo centered on the Galactic core, especially concentrated toward the Sagittarius–Scorpius–Ophiuchus

FIGURE 2.1: NGC 4147 is located about 60,000 light-years from Earth in the northern constellation of Coma Berenices (the Berenice's hair).
Credit: ESA/Hubble & NASA, T. Sohn et al.

region. Some of the most distant clusters, such as NGC 2419, lie far beyond the edge of the Galactic disk, up to distances of ∼300,000 light years. Radial velocity measurements show that most GCs follow highly elliptical orbits around the Galactic center, with periods on the order of 10^8 years or longer. During these orbits, they are subjected to various perturbations such as tidal forces, disk crossings, stellar escape, and internal dynamical evolution that may contribute to the eventual disruption of clusters over cosmic time.

It is estimated that many present-day GCs are survivors of a once larger population. Over the next 10 billion years, many may be lost. Notably, several clusters in Sagittarius (e.g., M54) are believed to be part of the Sagittarius Dwarf Elliptical Galaxy, which is currently merging with the Milky Way. Most Galactic GCs exhibit high relative velocities (100–300 km s^{-1}) with respect to the Sun and do not partake in disk rotation. However, a subset known as "disk globulars" shows properties consistent with the Galactic disk. Spectroscopic studies reveal that GC stars are typically metal-poor, confirming their origin during the Galaxy's early formation stages. This makes them powerful probes of the early universe.

Beyond the Milky Way, nearly all galaxies appear to host GC systems. M31 (Andromeda) has over 350 confirmed clusters. Massive ellipticals like M87 host thousands. Interestingly,

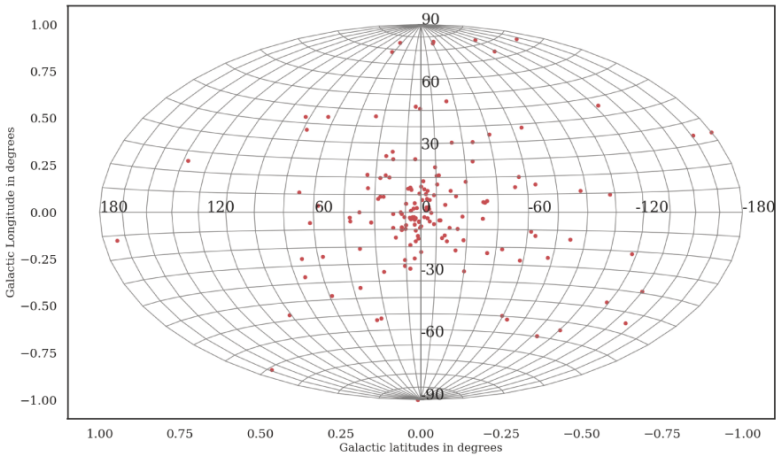

FIGURE 2.2: Distribution of globular clusters in the Milky Way in the catalog of Harris [5]. The clusters are concentrated around the centre of the galaxy.

some nearby galaxies such as the Magellanic Clouds and M33 contain much younger GCs (ages of a few Gyr or less), suggesting that cluster formation is still ongoing in certain environments. Modern observations also reveal that massive young star clusters possibly proto-GCs are forming in interacting galaxies. While their classification as true GCs is debated, their existence challenges the long-standing view that GCs are exclusively ancient, metal-poor systems.

2.1.1 Historical Background

The earliest human encounters with globular clusters likely date back to antiquity, when the naked eye could just glimpse ω Centauri, the largest known globular cluster in the Milky Way, low on the horizon in the southern hemisphere.

The first systematic astronomical detections began in the 18^{th} century. In the 1830s, John Herschel noted that a significant number of these clusters appeared to be concentrated in a relatively small region of the sky, specifically toward the constellation Sagittarius.

A major leap in understanding came in 1917 when HARLOW SHAPLEY studied variable stars in many globular clusters. Assuming these variables were Cepheid stars with known absolute magnitudes, he calculated distances to the clusters and, by extension, to the Galactic center. His pioneering work led to the realization that the center of the Milky Way lies far from the Sun in the direction of Sagittarius, and allowed him to estimate the size of the Milky Way.

Although Shapley's estimate was groundbreaking, we now know he significantly overestimated the size of both the Milky Way and the globular cluster system by a factor of two or more. This was primarily because the variable stars he studied were not Cepheids but rather *RR Lyrae* stars, which are intrinsically 2 to 4 magnitudes fainter than Cepheids.

2.1.2 The Key Role in Astronomy

Individual globular clusters, as well as entire GC systems, are valuable not only as specific astrophysical targets but also as powerful tools for understanding a broad range of astrophysical and cosmological problems. Their study remains a benchmark in the field and a major area of interest for the international astronomical community.

Members of a globular cluster share a common origin and differ primarily in their initial mass. Since they form a *simple stellar population* (coeval, chemically homogeneous, and relatively isolated), GCs provide ideal laboratories for testing stellar structure and evolution theories. Thanks to the large number of stars they contain, nearly all stages of stellar evolution are represented, including those with very short lifetimes (as short as 10^4 years), allowing direct comparisons with theoretical models.

Dynamically, globular clusters consist of around one million stars packed within a small volume, interacting through gravity. This makes them excellent environments for studying *stellar dynamics* and testing detailed theoretical dynamical models. When studied as a population, GCs serve as fossil tracers of the dynamical and chemical evolution of their host galaxies. They can be used as test particles to infer the total mass and the mass distribution of the parent galaxy.

Globular clusters also host a variety of interesting objects that warrant continuous investigation. These include strong and weak X-ray sources, neutron stars, millisecond pulsars, white dwarfs, cataclysmic variables, binary systems, blue stragglers, and planetary nebulae. They also contain one of the most important types of intrinsic variable stars, the RR Lyrae stars. These stars typically vary in brightness by less than two magnitudes and have periods ranging from 0.2 to 1.1 days. Since their mean absolute magnitude is fairly constant and only weakly dependent on metallicity (within 0.3 magnitudes), they serve as reliable *standard candles* for measuring astronomical distances.

Globular cluster research also has a profound impact on our understanding of cosmic chronology. GCs are among the oldest known objects in the Milky Way, and their ages can be estimated with relatively high precision. As they formed during the early stages of

Galactic evolution, they provide a firm lower limit to the age of the universe. Furthermore, their age distribution, and how it correlates with metallicity, spatial location in the Galaxy, and kinematics, offers insight into the timeline of star formation in the Galactic halo and supports broader theories of galaxy formation.

2.1.3 Color–Magnitude Diagrams

A Color-Magnitude Diagram (CMD) is a fundamental observational tool in stellar astrophysics that plots the brightness (magnitude) of stars against their color, which serves as a proxy for temperature. Typically, the vertical axis represents the visual magnitude, while the horizontal axis shows a color index, such as B–V. The CMD is similar to the Hertzsprung–Russell diagram but is based on observational data rather than theoretical quantities. It is widely used to study the structure and evolution of star clusters, especially globular clusters.

CMDs display key stellar evolutionary features such as the main sequence, red giant branch, and horizontal branch. In globular clusters, the main sequence is well-defined and extends from the turn-off point to fainter magnitudes and redder colors, reflecting stars that are fusing hydrogen into helium in their cores. The position of the main sequence turn-off is particularly important, as it provides an estimate of the cluster's age. In globular clusters, this turn-off occurs at fainter luminosities compared to nearby younger stars, indicating their ancient nature. CMDs are also used to determine distances, measure interstellar reddening, and distinguish cluster members from field stars, making them essential tools in the study of stellar populations and galactic evolution [6].

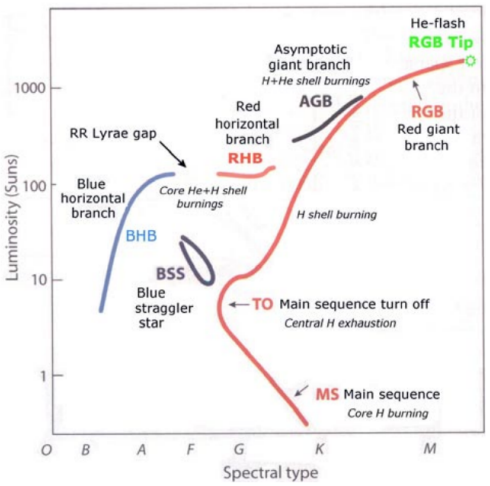

FIGURE 2.3: Color-magnitude diagram for a typical globular cluster.

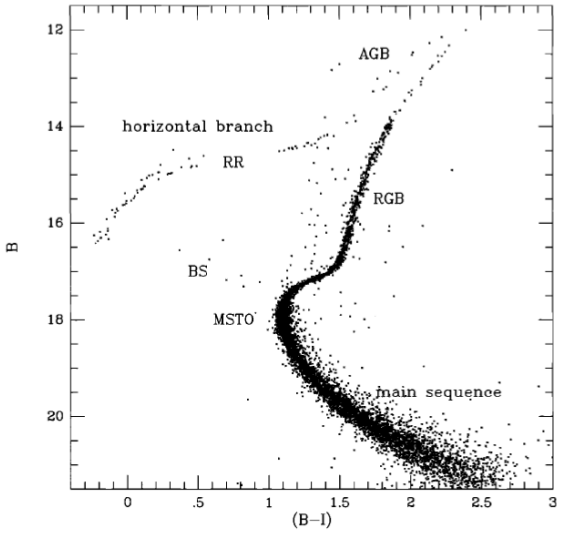

FIGURE 2.4: An observational form of the Hertzsprung-Russell diagram, showing the main sequence, turn-off point (MSTO), red giant branch (RGB), asymptotic giant branch (AGB), RR Lyrae gap, horizontal branch, and blue stragglers (BS) in a globular cluster [7].

2.1.3.1 Main Sequence

The main sequence in a CMD represents a continuous and prominent band of stars that are in the stable hydrogen-burning phase of stellar evolution. In globular clusters, the main sequence is well-defined and stretches from the brightest, bluest stars down to the faintest, reddest stars. A crucial feature of this sequence is the main-sequence turn-off point, where stars begin to exhaust hydrogen in their cores and evolve into later stages such as the red giant branch [8].

The position of this turn-off is a sensitive indicator of a cluster's age—older clusters have fainter and redder turn-offs, corresponding to lower mass stars ($\sim 0.8 M_\odot$), implying ages around 12–15 Gyr for typical Galactic globular clusters [9]. The narrowness of the main sequence in globular clusters reflects the fact that their stars formed nearly simultaneously and share a very similar chemical composition. Additionally, the position of the main sequence is influenced by metallicity: clusters with higher metallicity have redder and fainter main sequences at a given age, due to increased opacity from metal-rich stellar atmospheres [10]. The main sequence also has a theoretical lower mass limit around $0.08 M_\odot$, below which stars cannot sustain hydrogen fusion and are classified as brown dwarfs [6].

2.1.3.2 Red Giant Branch

The Red Giant Branch (RGB) is a prominent and crucial evolutionary phase in the CMD of globular clusters, representing the path followed by stars after they exhaust hydrogen in their cores. It extends from the subgiant region to brighter magnitudes and redder colors. During this phase, stars derive energy from hydrogen fusion occurring in a shell around an inert helium core, leading to the expansion and cooling of their outer layers. This results in increased luminosity and a redder color. The ascent continues until the ignition of helium in the degenerate core—the helium flash—marking the end of the RGB phase and the beginning of the horizontal branch [6].

In globular clusters, the RGB is typically narrow and well-defined, indicating a relatively uniform chemical composition among the stars. The morphology and location of the RGB in the CMD are influenced by metallicity: metal-rich clusters show redder and shallower RGBs, while metal-poor clusters exhibit bluer and steeper branches. This is due to increased opacity in metal-rich stellar atmospheres. The exact structure of the RGB is shaped by physical processes like mass-loss rates and convective mixing [11].

2.1.3.3 Horizontal Branch

The horizontal branch (HB) in a globular cluster's CMD represents stars that have evolved off the red giant branch and are now burning helium in their cores. These stars form a horizontal sequence in the CMD, typically bluer and of similar luminosity. The HB morphology, or the color distribution, is primarily influenced by metallicity and other stellar parameters [10].

A key HB population is the RR Lyrae stars, low-mass, metal-poor Population II stars located within the instability strip. Their stable absolute magnitudes and tight luminosity-metallicity relationship make them excellent standard candles for distance measurements. Metal-rich clusters (e.g., NGC 6637, $[\mathrm{Fe/H}] \approx -0.6$) tend to have redder HBs, while metal-poor clusters (e.g., NGC 1904, $[\mathrm{Fe/H}] \approx -1.7$) show bluer, more extended HBs [8, 7]. However, metallicity alone cannot explain HB diversity, leading to the second parameter problem.

Age is widely considered the second parameter: older clusters tend to have bluer HBs due to increased RGB mass loss. Yet, studies such as [9] suggest that age differences may not fully account for all variations, pointing to additional influences like helium abundance, CNO content, stellar rotation, or cluster density.

2.1.3.4 Asymptotic Giant Branch

The Asymptotic Giant Branch (AGB) represents a late evolutionary phase of low- to intermediate-mass stars (~ 0.8–$8M_{\odot}$), occurring after the exhaustion of helium in the core during the HB phase. Once the core helium is depleted, the star contracts again, and helium shell burning commences around an inert carbon-oxygen core, accompanied by a hydrogen-burning shell above it [6].

The simultaneous energy output from these two shells causes the star to ascend the giant branch for the second time, forming the AGB in the CMD of globular clusters. AGB stars exhibit several distinctive features, including thermal pulses or helium shell flashes. Furthermore, AGB stars undergo significant mass loss through stellar winds, enriching the interstellar medium with elements such as carbon and s-process elements. This mass loss leads to the eventual ejection of the stellar envelope, leaving behind a post-AGB star that will evolve into a white dwarf [12].

2.1.3.5 Blue Stragglers

Blue stragglers are an intriguing stellar population found in the CMDs of globular clusters. These stars appear as an extension of the main sequence beyond the cluster's main-sequence turn-off, suggesting they are hotter and more luminous than expected for their evolutionary stage [13].

Two primary formation mechanisms are proposed for blue stragglers: mass transfer in binary systems, and stellar collisions, especially in dense cluster cores. Observations suggest that both mass transfer and collisions contribute, with the dominant process depending on the environment [7].

2.2 Properties of Globular Clusters

2.2.1 Globular Cluster ages

Globular clusters are among the oldest stellar systems in the universe, with typical ages ranging from 10 to 13 billion years. The most reliable method for estimating globular cluster ages is by determining the mass and luminosity of stars at the main-sequence

turnoff point, a feature in the CMD [8]. This involves comparing observed data with theoretical stellar evolution models (isochrones).

Additional methods, such as white dwarf cooling sequences and nucleocosmochronology, serve as independent age indicators. Advances in trigonometric parallax data for subdwarfs have improved distance estimates, reducing one of the largest sources of uncertainty in these age determinations [6].

2.2.2 Chemical Properties

Globular clusters are often characterized by a remarkable degree of chemical homogeneity in their iron-peak element content, particularly [Fe/H], across member stars [14]. In contrast, they often show significant star-to-star variations in light elements such as C, N, O, Na, and Al.

Standard stellar evolution theory predicts that as a star ascends the RGB, its convective envelope deepens and dredges up material that has undergone CNO-cycle processing in the stellar interior. Observations support this, showing decreasing [C/H] and increasing [N/Fe] along the RGB in many clusters [11]. The observed trends, including the decline of $^{12}C/^{13}C$ with luminosity, suggest more mixing than standard models predict.

Interestingly, carbon depletion and associated mixing appear to be more efficient in metal-poor clusters than in metal-rich ones, a phenomenon predicted by meridional circulation models [10].

Chapter 3

Data and Methodology

3.1 Obtaining the raw data sample

The data used in this study has been obtained from Gaia Data Release 3 (DR3). Key parameters such as right ascension, declination, proper motion and its associated uncertainties, as well as photometric information (e.g., color and magnitude) for each star in the cluster were retrieved using the Astronomical Data Query Language (ADQL). The raw data sample, in general contains a large number of sources which do not fit the single stellar model or maybe are not part of the cluster itself or their photometric data is plagued by noise etc. We apply certain criterion to select stars which are astrometrically and photometrically well-behaved. In order to remove stars which are not a part of the cluster we apply a proper motion cut described later.

3.2 Cleaning the data-sets

To select astrometrically well-behaved sources, we applied the following criteria as recommended in the data release documentation and literature [15]:

1. **RUWE < 1.4**
   RUWE is the re-normalised unit weight error. This condition ensures that we use the stars whose astronomical observations are well fitted by a single-star model. Higher values may indicate some problematic or non-single sources.

2. **ASTROMETRIC_EXCESS_NOISE_SIG $\leq$ 2**
   Excess noise is the extra noise in each observation assumed to explain the residual scatter in the astrometric solution. If ASTROMETRIC_EXCESS_NOISE_SIG is greater than two, then this excess noise is statistically significant.

3. **ASTROMETRIC_GOF_AL $<$ 3**
   This parameter represents how good the fit is between the astrometric model and the observations. Higher values indicate a bad fit.

4. **VISIBILITY_PERIODS_USED $>$ 10**
   This parameter indicates the set of observations separated by at least 10 days. A higher value indicates that the source is well observed.

5. **0.001 + 0.039(BP−RP)** $<$ $\log_{10}$**(excess_flux)** $<$ **0.12 + 0.039(BP−RP)**
   Excess_flux is the corrected `phot_bp_rp_excess_factor` [16]. This factor can be estimated using the python code provided by [17]. The sources that are out of this range have inconsistent fluxes for various reasons, such as the presence of another nearby source, or the observed source may be an extended source.

Now, in order to select likely cluster members we use the cluster PM and PM dispersion taken from [15] and [5] respectively.
PM RA ($\overline{\mu_\alpha \cos\delta}$) $= -1.71$ mas yr^{-1}, $\quad \sigma_{\mu_\alpha \cos\delta} = 0.21$ mas yr^{-1}
PM DEC ($\overline{\mu_\delta}$) $= -2.08$ mas yr^{-1}, $\quad \sigma_{\mu_\delta} = 0.19$ mas yr^{-1}
RV (Heliocentric radial velocity) $= 183.2$ km s^{-1}

After applying the above conditions, we get the photometric data for a total of 2389 stars. Table 3.1 shows a sample of position and proper motion data extracted from Gaia DR3 for 5 stars. We began our analysis using the Gaia DR3 data for stars of NGC 4147, we selected only those stars which seemed to be the cluster members. To obtain these possible members, we selected stars based on the following criteria:

1. Proper motion of the star consistent with the proper motion of the cluster.
2. Consistent with the selection based on the membership probabilities.
3. Location in the color-magnitude diagram (CMD) consistent with the CMD of the cluster.

Only stars that met the aforementioned criteria were considered probable members of the cluster. These criteria were applied to all stars located within a radius extending up to five

TABLE 3.1: Proper motion and positional data for 5 stars in NGC 4147 extracted from Gaia DR3.

S.No	α (RA)	δ (Dec)	$\mu_\alpha \cos\delta$	μ_δ	$\sigma_{\mu_\alpha \cos\delta}$	σ_{μ_δ}
1	182.549859	18.539132	−2.066131	−0.994648	1.095702	0.872899
2	182.539023	18.533168	−2.165506	−2.731644	0.854342	0.599843
3	182.556507	18.556774	−1.910701	−2.036851	0.615011	0.467600
4	182.485128	18.570416	−1.926746	−1.412548	0.729234	0.675337
5	182.472899	18.572690	1.207729	−2.082758	1.248144	0.811114

times the tidal radius (r_t) of the cluster, as prescribed by [18]. Stars positioned between r_t and $5r_t$ from the center of the cluster were identified as extra-tidal candidates for further analysis. For this study, the adopted value of r_t is 6.6 arcmin, based on [1]. A detailed explanation of the implementation of these selection conditions is presented in Chapter 4.

Chapter 4

Data Analysis

We are going to identify the potential extra-tidal stars that were once members of the cluster. The selection analysis is based on the criteria discussed in the upcoming sections.

4.1 Proper Motion Selection

Proper motion is the astrometric measure of the observed changes in the apparent places of stars or other celestial objects in the sky, as seen from the center of mass of the Solar System, compared to the abstract background of the more distant stars.[19] According to the paper[15], the RA (right ascension) and DEC (declination) values for NGC 4147 are 182.5263°and 18.542°respectively. Also, the absolute proper motion for our cluster i.e. pmra ($\overline{\mu_\alpha \cos\delta}$) and pmdec ($\overline{\mu_\delta}$) are -1.71 mas yr^{-1} and -2.08 mas yr^{-1} respectively along with their dispersion $\sigma_{\mu_\alpha \cos\delta}$ and σ_{μ_δ} are 0.21 mas yr^{-1} and 0.19 mas yr^{-1} respectively. Now, in order to obtain likely cluster members we cut the sample of extracted data at those pmra and pmdec whose difference with cluster's proper motion lies in the range of three times of dispersion of cluster's proper motion, i.e.

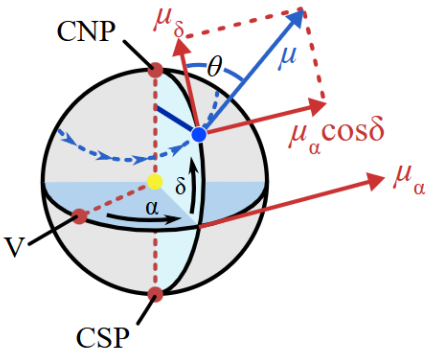

FIGURE 4.1: Representation of pmra ($\mu_\alpha \cos\delta$) and pmdec (μ_δ) on celestial sphere.[19]

$$\sqrt{\left(\mu_\alpha \cos\delta - \overline{\mu_\alpha \cos\delta}\right)^2 + \left(\mu_\delta - \overline{\mu_\delta}\right)^2} < 3\sqrt{\sigma^2_{\mu_\alpha \cos\delta} + \sigma^2_{\mu_\delta}} \tag{4.1}$$

In our whole study, we typically assume the behavior of extracted sample of our cluster as Gaussian distribution. Therefore, in Gaussian distribution 3σ encompasses the vast majority of data points (99.7%). This range represents the region where most "likely" data points are found. Values beyond this range are considered outliers or anomalies in a typical Gaussian distribution.

In this way, in our first step of selecting extra-tidal stars, we first select the central core of the data, which contains the majority of the "likely" members excluding outliers that fall outside the 3σ range, as they are considered to be highly unlikely under the Gaussian distribution. After cutting the sample, we get a total of 474 stars, which are most likely members of our cluster. Of these, 411 stars lie inside the tidal radius considered as cluster stars, and 63 are extra-tidal stars (stars lie outside the tidal radius). Figure 4.2 show these selected stars in the RA-DEC plane along with the tidal radius of the cluster.

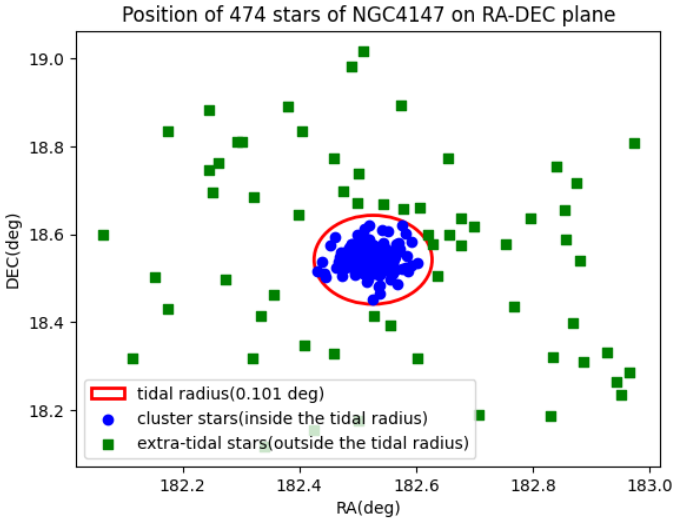

FIGURE 4.2: Position of stars on RA-DEC plane, compatible with proper motion of globular cluster NGC 4147

4.2 Membership Probability

Membership probability in globular clusters refers to the likelihood that a star observed near a cluster is actually a member of that cluster, rather than a field star passing through the same region of space. Analyzing membership probabilities is an extremely crucial

step in the process of selecting extra-tidal stars as this helps to identify which stars are genuinely part of the cluster's gravitational system.

In our study, we used the maximum likelihood method to obtain the membership probabilities of all stars selected by the proper motion criteria. Our approach is mainly based on the method described in[20] which was originally taken from[21]. The method is based on the Bayesian approach, which allows us to analyze the data against some hypothesis like whether the observed stars are cluster stars or field stars, in the context of our study on extra-tidal region of globular cluster. According to this approach, the probability distribution functions (p.d.f.) for cluster stars (ϕ_c^ν) and field stars (ϕ_f^ν) can be constructed for each star in the selected data as

$$\phi_c^\nu = \frac{1}{2\pi\sqrt{(\sigma_c^2+\epsilon_{xi}^2)(\sigma_c^2+\epsilon_{yi}^2)}} \times \exp\left\{-\frac{1}{2}\left[\frac{(\mu_{xi}-\mu_{xc})^2}{\sigma_c^2+\epsilon_{xi}^2}+\frac{(\mu_{yi}-\mu_{yc})^2}{\sigma_c^2+\epsilon_{yi}^2}\right]\right\} \tag{4.2}$$

$$\phi_f^\nu = \frac{1}{2\pi\sqrt{(1-\gamma^2)(\sigma_{xf}^2+\epsilon_{xi}^2)(\sigma_{yf}^2+\epsilon_{yi}^2)}} \times \exp\left\{-\frac{1}{2(1-\gamma^2)}\left[\frac{(\mu_{xi}-\mu_{xf})^2}{\sigma_{xf}^2+\epsilon_{xi}^2}-\frac{2\gamma(\mu_{xi}-\mu_{xf})(\mu_{yi}-\mu_{yf})}{\sqrt{(\sigma_{xf}^2+\epsilon_{xi}^2)(\sigma_{yf}^2+\epsilon_{yi}^2)}}+\frac{(\mu_{yi}-\mu_{yf})^2}{\sigma_{yf}^2+\epsilon_{yi}^2}\right]\right\} \tag{4.3}$$

where (μ_{xi}, μ_{yi}) are the proper motion of the ith star in the RA and Dec directions, $(\epsilon_{xi}, \epsilon_{yi})$ are observational errors in proper motion for the ith star, (μ_{xc}, μ_{yc}) are the mean proper motion of the cluster in the RA and Dec directions, which are mentioned earlier in Section 4.1, and σ_c is intrinsic dispersion of the cluster's proper motion, which we calculated from the equation $\sigma_c = \frac{\sigma_v}{R_{sun}}$, where σ_v is the central velocity dispersion and R_{sun} is the distance of the cluster NGC 4147 from the sun, taken as 0.00000265723093 pc yr^{-1} and 19300 pc respectively, from [5].

In the p.d.f. of field stars, (μ_{xf}, μ_{yf}) are the mean proper motion of the field stars in the RA and DEC directions, and $(\sigma_{xf}, \sigma_{yf})$ are the dispersion of the proper field motion. we have calculated these parameters using the Gaussian fit for field stars (here, the stars that lie outside the tidal radius are considered field stars), as shown in Figure 4.3. We plotted the proper motion ($\mu_\alpha \cos\delta$ and μ_δ) for field stars against the probability density, which is nothing but the p.d.f. of the Gaussian distribution, telling us about the likelihood density

at a particular value of proper motion ($\mu_\alpha \cos\delta$ and μ_δ). We have got

μ_{xf} = -1.67 mas yr^{-1} , σ_{xf} = 0.56 mas yr^{-1}

μ_{yf} = -2.19 mas yr^{-1} , σ_{yf} = 0.36 mas yr^{-1}

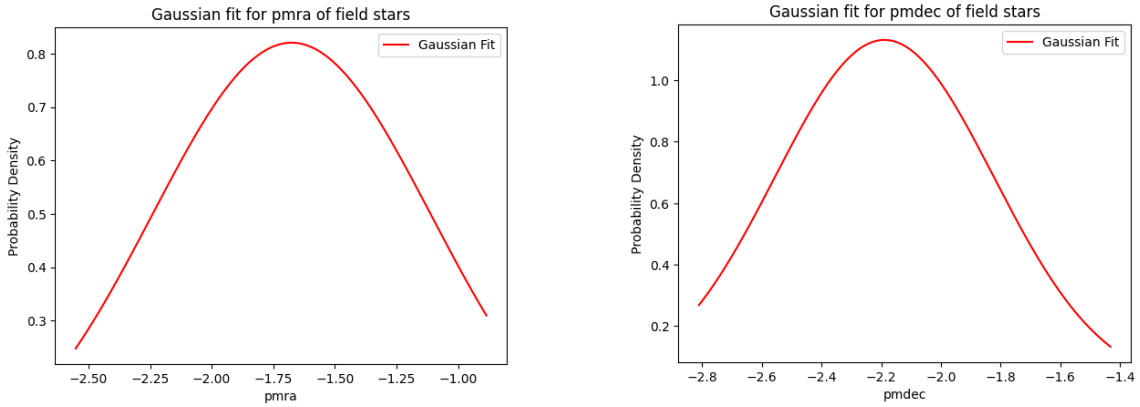

FIGURE 4.3: Gaussian fit for pmra ($\mu_\alpha \cos\delta$) and pmdec (μ_δ) of field stars.

Here, γ is the correlation coefficient which tells us the relation between the right ascension and the declination of the proper motion. This is important for calculating membership probability because stars that share similar proper motion vectors (both in right ascension and declination) are more likely to be part of the same cluster. It is defined as

$$\gamma = \frac{(\mu_{xi} - \mu_{xf})(\mu_{yi} - \mu_{yf})}{\sigma_{xf}\sigma_{yf}} \tag{4.4}$$

Now, the total distribution function (ϕ^ν) can be written as

$$\phi^\nu = n_c\phi_c^\nu + n_f\phi_f^\nu \tag{4.5}$$

where n_c and n_f are the normalized number of cluster stars and extra-tidal stars respectively in the selected sample obtained in Section 4.1. These are calculated as

n_c = 0.867 , n_f = 0.133

and therefore satisfies the relation: $n_c + n_f = 1$. Finally, the membership probability for ith star can be defined as

$$P(i) = \frac{n_c\phi_c^\nu}{\phi^\nu} \tag{4.6}$$

In this way, by calculating membership probability for each star in our selected sample, we found out that most of our selected extra-tidal stars have membership probability around 10% and beyond as shown in Figure 4.4. Therefore, we further select those extra-tidal stars, which have $P(i) \geq 0.1$, and this reduces our extra-tidal stars from 63 to 29.

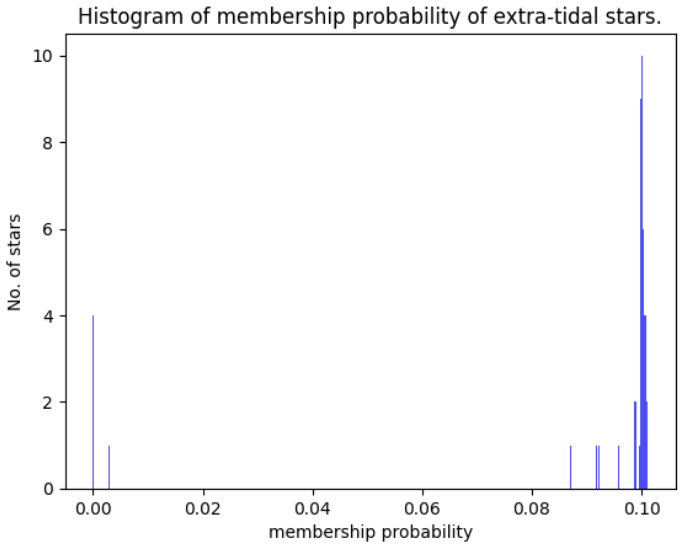

FIGURE 4.4: Histogram of Membership Probability for extra-tidal stars showing most of the stars have membership probability around 10%.

As of now, after the selection based on membership probability, we have 411 cluster stars and 29 extra-tidal stars, which gives us a total of 440 stars to carry our study further.

4.3 Color Magnitude Diagram

4.3.1 Correcting for extinction

The space between the radiation source and the observer is not completely empty but contains some interstellar medium, so part of the radiation if absorbed by the medium (and usually reemitted at a different wavelength, which maybe outside the band defining the magnitude), or scattered away from the line of sight. All these radiation losses are called the extinction.

4.3.1.1 Transformation and extinction corrected laws

The absolute magnitude (M) and the apparent magnitude (m) are connected by the equation,

$$m - M = 5 \log \left(\frac{r}{10\,\mathrm{pc}} \right) \tag{4.7}$$

where r is the distance of the source from the point of observation, But this equation is obtained by ignoring the radiation losses due to the interstellar medium. When we

consider these effects 4.7 gets modified to

$$m - M = 5 \log \left(\frac{r}{10\,\mathrm{pc}} \right) + (2.5 \log e)\, \tau \tag{4.8}$$

or

$$m - M = 5 \log \left(\frac{r}{10\,\mathrm{pc}} \right) + A \tag{4.9}$$

where $A = (2.5 log e)\tau$. This formula when applied to the gaia bands gives us,

$$B = M_B + 5 \log_{10} \left(\frac{r}{10\,\mathrm{pc}} \right) + A_B \tag{4.10}$$

where B and M_B are the apparent and absolute magnitudes in the blue band.

Similarly, for the red band:

$$R = M_R + 5 \log_{10} \left(\frac{r}{10\,\mathrm{pc}} \right) + A_R \tag{4.11}$$

The observed color index is given by:

$$B - R = (M_B - M_R) + (A_B - A_R) \tag{4.12}$$

or more compactly, Equation 4.12 may be written as:

$$B - R = (B - R)_0 + E_{B-R} \tag{4.13}$$

where $(B-R)_0$ is the intrinsic color of the celestial object and $E_{B-R} = (B-R) - (B-R)_0$ is the color excess. Now in order to transform from one color to another we use the polynomial equation

$$G_{BP-RP} = c_0 + c_1(B - V) + c_2(B - V)^2 + c_3(B - V)^3 \tag{4.14}$$

Studies of the interstellar medium show that the ratio of the visual extinction A_v (Absolute visual magnitude) to the colour excess E_{B-V} is almost constant for all stars, i.e.

$$\frac{A_v}{E_{B-V}} \approx 3 \tag{4.15}$$

Using the above equation we obtain the absolute magnitude in green band (G_{mag}) by estimating the extinction coefficient for green band (A_G) from the relation [22]

$$\frac{A_G}{A_V} = 0.83627 \tag{4.16}$$

where the value of E_{B-V} has already been obtained. On multiplying eq 4.15 and 4.16, we get

$$A_G \approx 2.50881 E_{B-V} \tag{4.17}$$

Once A_G is obtained we use the equation of the form 4.10 to get the intrinsic G magnitude of the object. The equation [23] used for extinction correction is,

$$G_0 = G - R_G \times 3.1 \times E(B-V) \tag{4.18}$$

$$(G_{BP} - G_{RP})_0 = (G_{BP} - G_{RP}) - (R_{BP} - R_{RP}) \times 3.1 \times E(B-V) \tag{4.19}$$

where,

$$R_G = 2.726$$
$$R_{BP} = 3.310$$
$$R_{RP} = 2.009$$
$$E(B-V) = 0.02$$

The coefficients for Gaia band passes were obtained from the [24] & the E(B-V) value from [5]. Table 4.1 shows the sample of color-magnitude data extracted from Gaia DR3 for 5 stars.

TABLE 4.1: Color-Magnitude data for five stars in NGC 4147 obtained from Gaia DR3.

S No.	G	G_{BP}	G_{RP}	$G_{BP} - G_{RP}$
1	20.225628	20.438187	19.793797	0.644390
2	19.926857	20.224590	19.616734	0.607857
3	19.810244	20.088234	19.513187	0.575047
4	21.047251	20.802969	20.768568	0.034401
5	20.858648	20.655558	20.890247	-0.234690

4.3.2 CMD for Globular Cluster NGC 4147

The Color Magnitude Diagram (CMD) of NGC 4147 was constructed using the Gaia DR3 photometry data for only selected stars in Section 4.2 as mentioned in Table 4.1. After applying the extinction correction as mentioned in Section 4.3.1.1 to remove the obscurence present in our data due to the atmosphere, we get the CMD of our cluster NGC 4147 as shown in Figure 4.5.

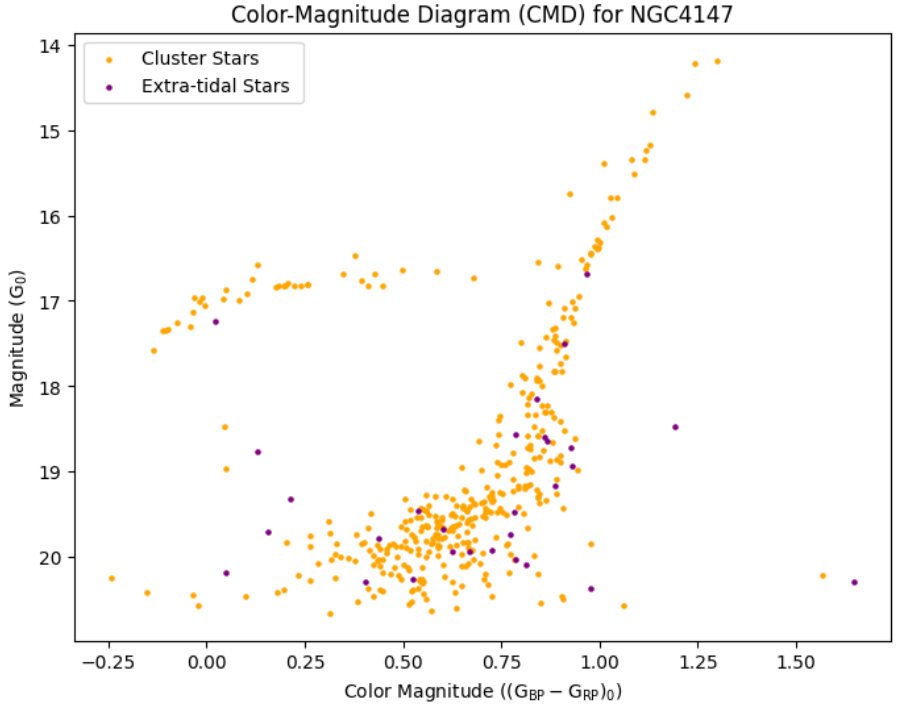

FIGURE 4.5: Color Magnitude Diagram for NGC 4147.

As we can see, it is a scatter plot of color magnitudes, which is, in this case, extinction-corrected $G_{BP} - G_{RP}$ magnitudes ($(G_{BP} - G_{RP})_0$) on the x-axis with luminosity magnitudes G_0 (extinction-corrected G magnitudes) on the y-axis. The color magnitudes are the proxy for temperature, and the luminosity magnitudes are the proxy for luminosity. Also, brighter stars are plotted at the top, and hotter (bluer) stars are plotted on the left, as the G magnitudes on the y axis are generally plotted inversely in the CMD.

In the NGC 4147 CMD in Figure 4.5, we can clearly see that there is no main sequence left on the CMD and only a red giant branch with a red turn-off point is seen, which indicates that the cluster is very old, as it should. A horizontal branch can also be seen on the CMD with some gaps that can indicate the presence of RR Lyrae variable stars. The more detailed explanation of these branches is already mentioned in Chapter 2.

By performing the Isochrone fitting in Section 4.4, we can further select the most likely extra-tidal candidates.

4.4 Isochrone Fitting

To analyze the stellar population of the globular cluster NGC 4147, we performed isochrone fitting using models from the PARSEC stellar evolution database [25]. Isochrone fitting is a method of comparing theoretical predictions for stellar evolution with observed color magnitude diagrams (CMDs), to estimate key physical parameters of a star cluster, such as age, metallicity, and distance.

4.4.1 Isochrone Models

We selected several isochrone models from the PARSEC database, each with varying combinations of:

- Age (in log(Age/yr))
- Metallicity ([Fe/H])

Each isochrone represents the expected distribution of stars for a stellar population with a specific chemical composition and formation time. The models include absolute magnitudes in the Gaia bands (G, G_{BP} and G_{RP}), which are then corrected for extinction and adjusted using a distance modulus during fitting, as mentioned in Section 4.3.1.1.

4.4.2 Fitting Methodology

Each isochrone was tested against the observed CMD of NGC 4147 by applying a trial distance modulus (DM) and minimizing the average squared distance between the isochrone and the cluster stars in CMD space. The procedure is as follows:

1. For each isochrone, correct its Gaia magnitudes for extinction and shift the magnitude axis using a trial distance modulus (DM):

$$G_{\text{fit}} = G_0 + DM \tag{4.20}$$

2. Define a cost function based on the average nearest-neighbor squared distance from each isochrone point to the closest observed cluster star as

$$\chi^2 = \frac{1}{N} \sum_i \min_j \left[(c_i - c_j)^2 + (m_i - m_j)^2 \right] \tag{4.21}$$

where (c_i, m_i) are isochrone color–magnitude pairs and (c_j, m_j) are observed stars.

3. Alternatively, this can be expressed using a direct comparison metric in CMD space:

$$\text{Distance}^2 = \min \left[(G_0^{\text{obs}} - (G_0^{\text{iso}} + DM))^2 + ((BP - RP)_0^{\text{obs}} - (BP - RP)_0^{\text{iso}})^2 \right] \tag{4.22}$$

4. Use numerical optimization (via `scipy.optimize.minimize` from SciPy [26]) to determine the best-fit distance modulus for each isochrone.

The isochrone with the lowest value of χ^2 is considered the best fit. This approach avoids binning and directly compares continuous distributions, making it robust against CMD resolution effects.

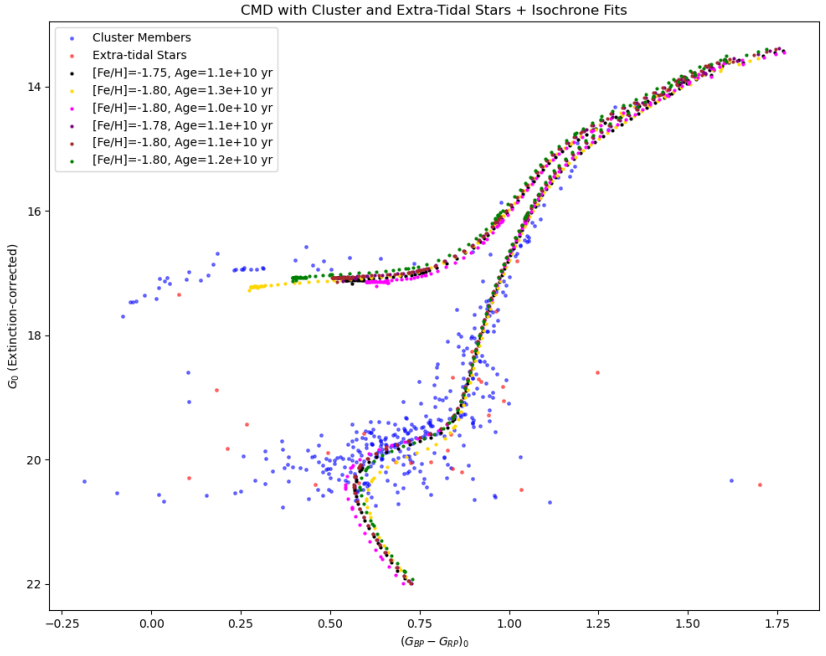

FIGURE 4.6: Color–magnitude diagram of NGC 4147 with several PARSEC isochrone models of different ages and metallicities overplotted.

4.4.3 Best Fit Isochrone Selection

Each isochrone model yields a fit score based on the average distance between the model and data points in CMD space (analogous to a reduced chi-square),

$$\chi^2_{\text{iso}} = \text{average CMD distance for a given isochrone} \tag{4.23}$$

We selected the best-fit isochrone as the one with the lowest fit score χ^2_{iso} (Equation 4.22). This method assumes that the closest visual match in the CMD space reflects the most accurate physical model for the cluster.

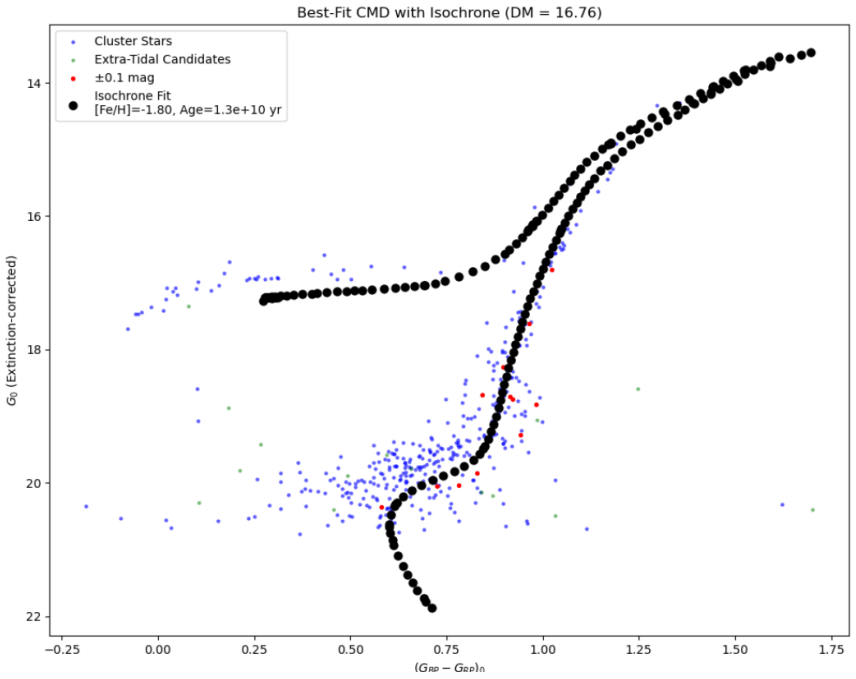

FIGURE 4.7: Best-fit isochrone model selected by minimizing the average distance in CMD space.

4.4.4 Identifying Extra-Tidal Candidates

After selecting the best-fitting isochrone, we identify those extra-tidal stars (located beyond the tidal radius of NGC4147), that closely follow the same evolutionary sequence. Therefore, already selected extra-tidal stars in Section 4.2 are compared with the best-fit isochrone, and those within ±0.1 mag in both color and magnitude are flagged as potentially most likely extra-tidal stars associated with the globular cluster NGC4147. This approach enables a more physically motivated selection than simple radial cuts, as it incorporates stellar evolutionary information from the color–magnitude diagram.

Using this method, a total of **14** extra-tidal stars were found to lie along the best-fit isochrone, suggesting that they may be the most genuine cluster members dispersed beyond the nominal tidal boundary.

4.5 Estimation of Age and Metallicity

The best-fitting isochrone directly provides estimates of the cluster's:

- **Age**, inferred from the position of the main sequence turnoff and subgiant branch. From the best-fit model, the age of NGC 4147 is estimated to be $(1.3 \pm 0.2) \times 10^{10}$ years, compared to [27].
- **Metallicity**, inferred from the slope and shape of the red giant branch and other CMD features. The corresponding metallicity is found to be [Fe/H] $= -1.8$ dex, which is consistent with the results in [27].

The success of the model in matching the CMD structure, including the main sequence, the red giant branch, and the horizontal branch, supports the derived parameters. For NGC 4147, this process confirms that it is an old, metal-poor globular cluster, which is consistent with previous studies.[15]

4.6 Density Plot

The density map of the selected extra-tidal candidates ($N_{extra-tidal}$), along with the proper motion direction of the cluster(blue line), and r_t and $5r_t$ of the cluster is illustrated in Figure 4.8, where a total of 14 extra-tidal star candidates are indicated. The density maps were created using the kernel density estimator (KDE) routine of the scipy module [28]. The bandwidth used for Gaussian KDE is 7.43 arc min [15]. Here, ΔRA is the difference between the RA of the extra-tidal star and the RA of the cluster, the same as for ΔDec. The figure also shows the direction towards the galactic center (red line) and the orbit followed by the cluster in the future (orange line). The inner white circle and outer dark grey circle correspond to r_t and $5r_t$, respectively. The contour lines represent the iso-density regions with a constant number of stars per square degree [15].

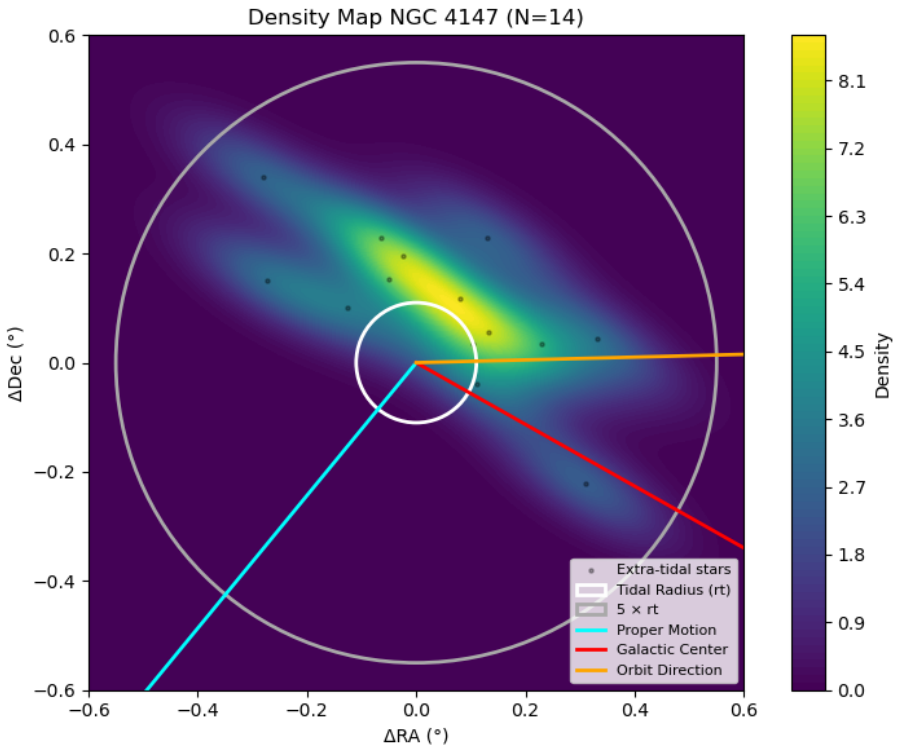

FIGURE 4.8: Density Map of the selected extra-tidal candidates (black dots), along with the PM (blue) of the cluster, r_t (white), $5r_t$ (dark grey), the direction of the galactic center (red line) and the orbit of the cluster in the future(orange line).

4.7 Orbit of the Cluster

At the epoch J2000, the galactic longitude and latitude of the cluster are 252.85° and +77.19°, respectively. The orbit of the cluster was obtained using the GravPot16 web interface [29]. Figure 4.9 shows the cluster's orbit projected in the R–Z and X–Y planes. It is evident from the plots that NGC 4147 moves up to 20 kpc above and below the Galactic plane. These large vertical motions suggest that the cluster repeatedly crosses the disk, experiencing gravitational interactions known as disk and bulge shocks. Over time, such interactions can strip stars from the cluster's outer regions. The extra-tidal features observed today may therefore be remnants of this process, shaped by long-term tidal forces and the Milky Way's gravitational field.

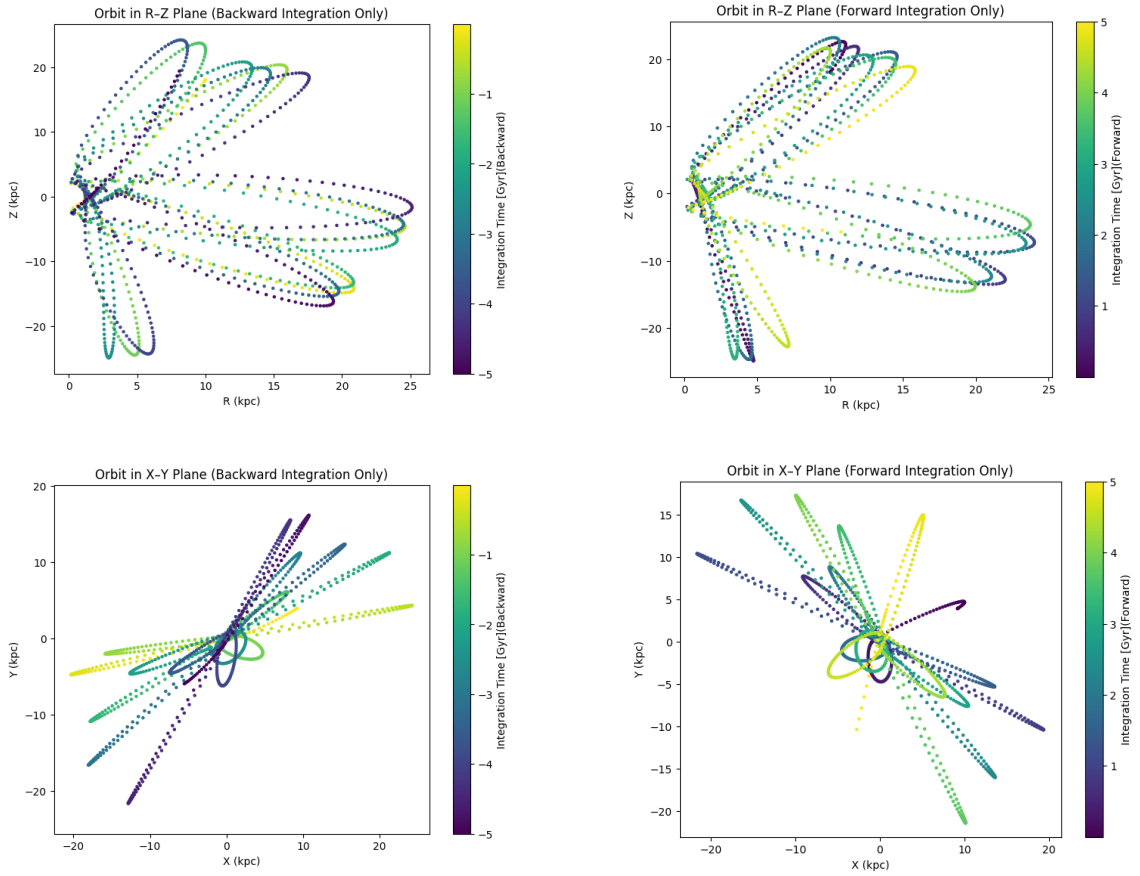

FIGURE 4.9: Orbit of NGC 4147 in the R–Z (top) and X–Y (bottom) planes. Each pair shows backward and forward integrations over 5 Gyr.

Chapter 5

Results

In our study of the extra-tidal region of NGC 4147, along with the estimation of its age and metallicity, we have found the age of the cluster and metallicity around $(1.3 \pm 0.2) \times 10^{10}$ years and -1.8 dex, respectively. These results are purely based on the study of the cmd of the cluster and isochrone fitting. The estimated age and metallicity of NGC 4147 are consistent with earlier studies on the globular cluster NGC 4147.

In the context of the extra-tidal region of the globular cluster NGC 4147, we started the process of selecting extra-tidal stars with a total of 2389 stars' photometric data, and after the detailed selection process, we get a total of 425 stars. Of these, 411 are cluster stars and 14 are finally considered the most likely extra-tidal candidates after isochrone fitting. But this list of extra-tidal candidates cannot be considered as complete as we may have lost some genuine candidates along the way. Also, the reason for getting such a small number of extra-tidal stars is that some loosely bound stars already left the cluster in the past and currently lie outside the region of $5r_t$ of the globular cluster; hence they are not considered as extra-tidal stars.

In addition, we can see the density plot of these selected extra-tidal stars in Figure 4.8, which shows the overdensity of these stars in the opposite direction to that of the proper motion of the cluster, which indicates that the bulge or disk shocks have been experienced by the cluster from the host galaxy, in this case the Milky Way. In addition to the density plot, the orbits of our cluster as shown in Figure 4.9 indicates that the cluster NGC 4147 has passed through the Galactic disk many times and will continue to do so in the future. This is the possible reason for shocks experienced by the cluster, which results as the tidal disruption by the matter in the galactic disk leads to the presence of extra-tidal stars in the cluster.

Chapter 6

Conclusion

We estimated the age, metallicity and analyzed the extra-tidal region of NGC 4147. Extra-tidal candidates were selected based on the proper motion of the cluster and the stars, and the position of the stars on the isochrone fitted CMD of the cluster. The mean proper motions and dispersions for cluster and field stars were estimated using literature values and a Gaussian model, respectively. Notably, stars located opposite to the direction of the cluster's proper motion appear more dispersed, suggesting they may be more strongly affected by the gravitational potential of the Milky Way.

To conclude, the candidates identified in this study represent the most probable extra-tidal members based on currently available Gaia astrometry and photometry data. However, a definitive confirmation requires follow-up star-by-star analysis of their radial velocity measurements.

Bibliography

[1] Julio A. Carballo-Bello, Antonio Sollima, David Martínez-Delgado, Berenice Pila-Díez, Ryan Leaman, Jürgen Fliri, Ricardo R. Muñoz, and Jesús M. Corral-Santana. A search for stellar tidal debris of defunct dwarf galaxies around globular clusters in the inner galactic halo. *Monthly Notices of the Royal Astronomical Society*, 445(3):2971–2993, October 2014.

[2] Wikipedia contributors. Globular cluster. `https://en.wikipedia.org/wiki/Globular_cluster`, 2025. Accessed: 2025-04-08.

[3] Richa Kundu, Camila Navarrete, José G. Fernández-Trincado, Dante Minniti, Harinder P. Singh, Luca Sbordone, Andrés E. Piatti, and Céline Reylé. The search for extratidal star candidates around galactic globular clusters ngc 2808, ngc 6266, and ngc 6397 with gaia dr2 astrometry. *Astronomy & Astrophysics*, 645:A116, 2021.

[4] Wikipedia contributors. Ngc 4147. `https://en.wikipedia.org/wiki/NGC_4147`, 2025. Accessed: 2025-04-08.

[5] W. E. Harris. A catalog of parameters for globular clusters in the milky way (2010 edition). `https://www.physics.mcmaster.ca/~harris/mwgc.dat`, 1996. AJ, 112, 1487. The catalog is periodically updated; use the 2010 edition.

[6] B. W. Carroll and D. A. Ostlie. *An Introduction to Modern Astrophysics*. Cambridge University Press, 2017.

[7] K. M. Ashman and S. E. Zepf. *Globular Cluster Systems*. Cambridge University Press, 1998.

[8] D. A. VandenBerg, M. Bolte, and P. B. Stetson. Constraints on globular cluster ages and distance scales from theoretical isochrones. *Annual Review of Astronomy and Astrophysics*, 34:461–510, 1996.

[9] P. B. Stetson, D. A. VandenBerg, and M. Bolte. The ages of globular clusters in the halo of the galaxy. *Publications of the Astronomical Society of the Pacific*, 108(723):560–578, 1996.

[10] R. G. Gratton, C. Sneden, and E. Carretta. Abundance variations within globular clusters. *Annual Review of Astronomy and Astrophysics*, 38:241–289, 2000.

[11] R. P. Kraft. Abundance differences among globular cluster giants: Primordial vs. evolutionary scenarios. *Publications of the Astronomical Society of the Pacific*, 106:553–565, 1994.

[12] J. G. Cohen. Mass loss from red giants in globular clusters. *The Astrophysical Journal*, 203:L127–L130, 1976.

[13] C. D. Bailyn. Blue stragglers as evidence for dynamical interactions in globular clusters. *Annual Review of Astronomy and Astrophysics*, 33:133–162, 1995.

[14] E. Carretta and R. G. Gratton. Abundances of globular cluster stars: iron content and alpha-element enhancements. *Astronomy and Astrophysics Supplement Series*, 121:95–112, 1997.

[15] Richa Kundu, Camila Navarrete, Luca Sbordone, Julio A. Carballo-Bello, José G. Fernández-Trincado, Dante Minniti, and Harinder P. Singh. Extra-tidal star candidates in globular clusters of the sagittarius dwarf spheroidal galaxy. *Astronomy amp; Astrophysics*, 665:A8, August 2022.

[16] M. Riello, F. De Angeli, D. W. Evans, P. Montegriffo, J. M. Carrasco, et al. Gaia early data release 3: Photometric content and validation. *Astronomy & Astrophysics*, 649:A3, May 2021.

[17] A. G. A. Brown, A. Vallenari, T. Prusti, J. H. J. de Bruijne, C. Babusiaux, et al. Gaia early data release 3: Summary of the contents and survey properties (corrigendum). *Astronomy & Astrophysics*, 650:C3, 2021.

[18] Ivan King. The structure of star clusters. I. an empirical density law. , 67:471, October 1962.

[19] Wikipedia contributors. Proper motion, 2025. Accessed: 2025-04-09.

[20] D. P. Sariya, R. K. S. Yadav, and A. Bellini. Proper motions and membership probabilities of stars in the region of globular cluster ngc 6809. *Astronomy & Astrophysics*, 543:A87, 2012.

[21] L. Balaguer-Núñez, C. Jordi, D. Galadí-Enríquez, and J. L. Zhao. New membership determination and proper motions of ngc 1817. parametric and non-parametric approach. *Astronomy & Astrophysics*, 426:819–826, 2004.

[22] P. Marigo, L. Girardi, A. Bressan, P. Rosenfield, B. Aringer, Y. Chen, M. Dussin, A. Nanni, and G. Pastorelli. A new generation of parsec-colibri stellar isochrones including the tp-agb phase. *The Astrophysical Journal*, 835(1):77, 2017. CMD 3.8 input form, PARSEC-COLIBRI isochrones. Accessed April 2025.

[23] Henri M.J. Boffin. Colour-magnitude diagrams. `https://www.eso.org/~hboffin/Teaching/CMD.html`, n.d. Accessed: 2025-04-10.

[24] L. Casagrande, J. Lin, A. D. Rains, F. Liu, S. Buder, J. Horner, M. Asplund, G. F. Lewis, S. L. Martell, T. Nordlander, D. Stello, Y.-S. Ting, R. A. Wittenmyer, J. Bland-Hawthorn, A. R. Casey, G. M. De Silva, V. D'Orazi, K. C. Freeman, M. R. Hayden, ..., and T. Zwitter. The galah survey: Effective temperature calibration from the infrared flux method in the gaia system. *Monthly Notices of the Royal Astronomical Society*, 507(2):2684–2696, 2021.

[25] PARSEC, CMD Web Tool. Cmd 3.8 - web interface. `https://stev.oapd.inaf.it/cgi-bin/cmd`, 2025.

[26] Pauli Virtanen, Ralf Gommers, Travis E. Oliphant, and et al. SciPy 1.0: Fundamental algorithms for scientific computing in python. *Nature Methods*, 17:261–272, 2020.

[27] Ying-Hua Zhang, Jundan Nie, Hao Tian, and Chao Liu. Assessing the association between the globular cluster ngc 4147 and the sagittarius dwarf galaxy. *The Astronomical Journal*, 168(6):237, 2024.

[28] P. Virtanen, R. Gommers, T. E. Oliphant, and et al. Scipy 1.0: Fundamental algorithms for scientific computing in python. *Nature Methods*, 17(3):261–272, 2020.

[29] J. G. Fernandez-Trincado, A. C. Robin, C. Reylé, and O. Valenzuela. GravPot16: A Galactic potential model. `https://gravpot.utinam.cnrs.fr/`, 2016. Accessed: 2025-04-13.

[30] George Djorgovski. Globular clusters: A short overview. `https://sites.astro.caltech.edu/~george/ay20/eaa-globcl.pdf`, 2002. Accessed: April 10, 2025.